Progress In Electromagnetics Research C, Vol. 115, 41–50, 2021

A 28 GHz Surface-Mount Endfire Antenna Based on Ball Grid Array Packaging for 5G New Radio

Xiubo Liu[1], Wei Zhang[1], Dongning Hao[1], and Yanyan Liu[2, *]

Abstract—In this article, a 28 GHz endfire antenna based on ball grid array (BGA) packaging is proposed for the 5G mmWave new radio (NR). The antenna is composed of a pair of dipole patches fed by a substrate integrated waveguide (SIW). Besides, quasi-coaxial vertical transition and transition from grounded coplanar waveguide (GCPW) to SIW are designed on the substrate to achieve compact size. The substrate is based on a single-layer printed circuit board (PCB), which can meet the cost-effectiveness requirements of the 5G application. Meanwhile, the proposed antenna can be easily integrated with other surface-mount devices by using the BGA packaging. In particular, it can be mounted near the RF front-end chipset to improve system performance. Finally, the prototype is manufactured and verified. Experimental results show that the −10 dB bandwidth of the proposed antenna is 5.35% in the range of 27.3 to 28.8 GHz, and the peak gain achieves 4.4 dBi at 29 GHz.

1. INTRODUCTION

The 5G millimeter-wave (mmWave) communication enables high carrier frequency and broadband bandwidths to replace the crowded sub-3 GHz spectrum [1, 2]. The use of beamforming solutions can overcome the challenge of high path loss, rain attenuation, and atmospheric absorption in the mmWave frequency band. At the same time, the massive base station and device density require the use of dozens to hundreds of antenna elements in the phased array [3–7]. Therefore, the requirements for the 5G mmWave antennas are energy and cost-effectiveness, easy integration, and compact size.

A large amount of research on the 5G mmWave antenna has been reported [8–13]. Some magnetoelectric dipole antennas are introduced in [8] and [9]. A small and compact Huygens source antenna is presented in [10]. In [11], a titled radiation antenna toward 5G communication is introduced. A high radiation efficiency Vivaldi antenna based on an all-metallic structure is shown in [13]. The performance of the above antennas is good. However, the interconnection between the RF front-end chipset and the above-mentioned antennas must use lossy waveguide connectors or coaxial connectors. On one hand, the connectors may cause more insertion loss and reduce the system performance. On the other hand, it is very difficult to integrate with an RF system.

The advanced packaging and Antenna-in-Package (AiP) technology can integrate active front-end devices and passive components in the same module. The antenna can be placed very close to the RF front-end chipset to reduce insertion loss and improve system performance. Compared with the wire-bonding interconnection technique, the surface-mount devices using the flip-chip interconnection technology can reduce the parasitic effect and obtain better electrical performance by using the smaller solder balls, bumps, or pillars [14–16]. Many materials can be applied to AiP technology. For example, metal-based [17, 18], organic laminates [10, 19–21], low-temperature cofired ceramic [22–25], glass-based substrate [26], and silicon-based substrate [27]. The mentioned antennas can be integrated with

Received 5 July 2021, Accepted 12 August 2021, Scheduled 19 August 2021

* Corresponding author: Yanyan Liu (lyytianjin@nankai.edu.cn).

[1] School of Microelectronics, Tianjin University, Tianjin 300072, China. [2] Tianjin Key Laboratory of Photo-electronic Thin Film Devices and Technology, Nankai University, Tianjin 300071, China.

active chips into the same package. Among the above-mentioned antennas, antennas based on organic laminates have the advantages of low cost and good performance. However, the multi-layer structure is complicated and increases the cost.

Hence, this article proposes a low-cost single-layer endfire antenna using the ball grid array packaging technology. Owing to the single substrate layer, the proposed antenna achieves a desired cost-effective feature. Besides, the BGA packaging makes the antenna compact and realizes surface mount function. The proposed antenna has been designed, fabricated, and measured. The S-parameters and far-field radiation patterns are verified. The whole paper is organized as follows. Section 2 introduces the SiP configuration of the proposed antenna. Section 3 illustrates the detail of the antenna design. Section 4 discusses the experimental results. Finally, the conclusion is summarized in Section 5. In this article, the simulation results are given by the full-wave electromagnetic simulation software ANSYS HFSS.

2. PACKAGE AND ANTENNA STRUCTURE

The system-in-package (SiP) configuration of the proposed antenna is shown in Figure 1. The antenna integrates a dipole radiator and reflector. Compared to the Yagi-Uda antenna, for the sake of miniaturization, no director is added to the antenna. It can be seen that the proposed antenna can be easily surface mounted on the system laminate. Furthermore, it can be integrated with other high-performance discrete surface-mounted devices (SMD) by surface-mount technology (SMT). A multi-layered AiP may include DC signal layers that cost more. Unlike the multilayer AiP, the proposed antenna contains only a single-layer substrate, and the DC signals are placed on the system lamination. Therefore, the single-layer configuration is a good solution for cost reduction. Similarly, the antenna can be placed very close to the RF front-end chipset to reduce the insertion loss (L_c). As shown in Equation (1), the equivalent isotopically radiated power (EIRP) can be calculated as follows [28],

$$EIRP = P_T - L_C + G_a \tag{1}$$

where P_T is the output power of the transmitter; L_c is the insertion loss between the transmitter and the antenna; G_a is the antenna gain. As can be seen from Figure 1, the proposed antenna can be placed very close to the RF front-end chipset. The low-loss interconnection between the antenna and the RF front-end chip improves the EIRP and reduces the noise of the receiving channel. Finally, this configuration improves the performance of the RF system.

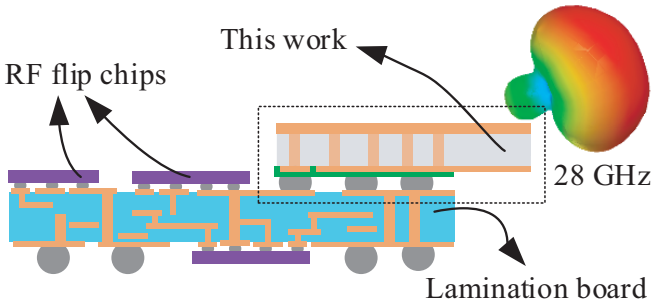

Figure 1. SiP configuration of the proposed antenna.

3. ANTENNA DESIGN

3.1. Antenna Element Configuration

As depicted in Figure 2, the antenna element is fabricated on a Rogers4350B substrate with a relative dielectric constant of 3.66, a dielectric loss tangent of 0.004, and a thickness of 0.254 mm. The dipoles are mirrored on the top and bottom layers. Additionally, the dipoles rotate 60 degrees to minimize the size. The dipoles are fed by a differential signal with equal amplitude and a differential phase. The

transmission from SIW to the GSG is carried out by a taper RF transition. The RF plated through holes (PTHs) connect the GSG to the bottom-feeding point with the resin plugging process. Another PTH connects the top grounded metal to the bottom metal. The RF PTH and grounded PTH form a vertical quasi-coaxial RF transition. Besides, an annular air gap insulates the RF feeding point from the grounded metal layer. Then, 300 µm Tin-Lead solder balls are mounted on the bottom layer. The input impedance of the RF feed point at the bottom layer is 50 Ω, so it can be easily connected to the RF chipset. The detailed values of the proposed antenna are listed in Table 1. The dimension of the antenna element is 5.9 mm × 3.4 mm × 0.6 mm.

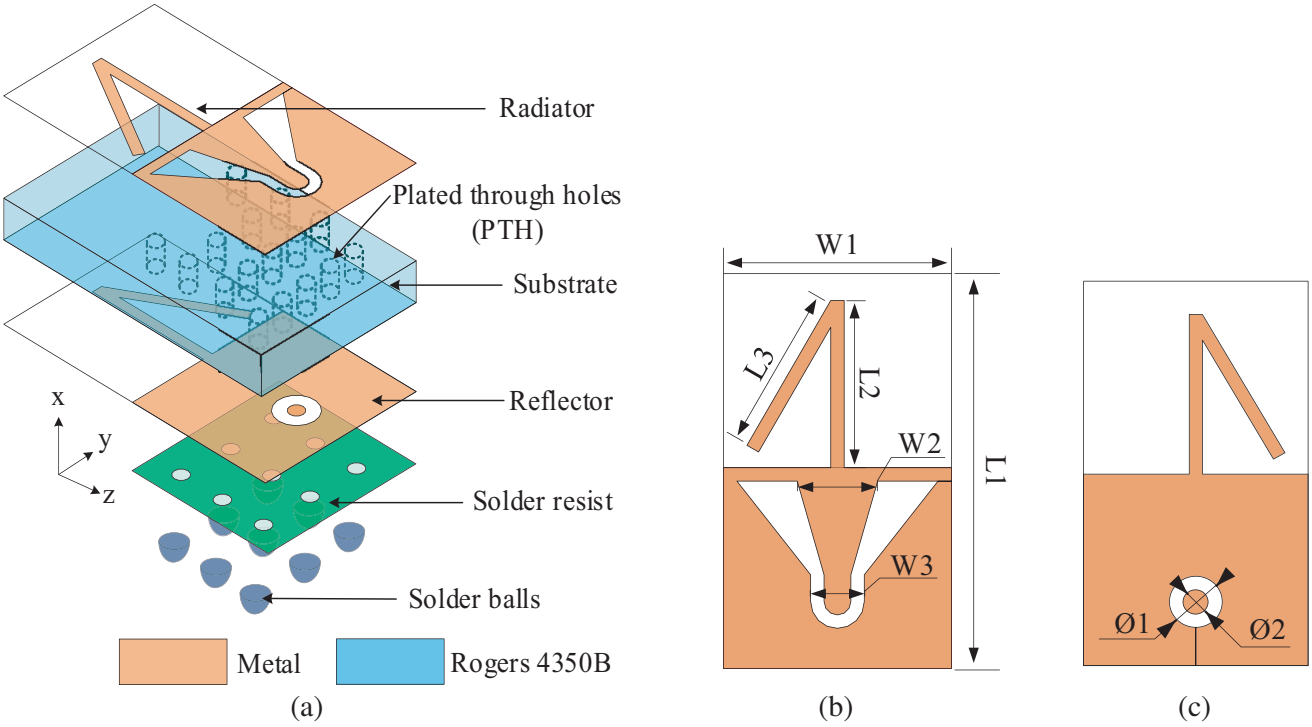

Figure 2. Geometry of the proposed antenna element. (a) Exploded view. (b) Top view. (c) Bottom view.

Table 1. Dimensions of the proposed antenna element (UNITS: mm).

Parameters	Values	Parameters	Values
$L1$	5.9	$W2$	1.2
$L2$	2.5	$W3$	0.8
$L3$	2.5	$\Phi 1$	0.8
$W1$	3.4	$\Phi 2$	0.3

The simulated antenna gain and efficiency of the antenna element are shown in Figure 3. It can be observed that the efficiency of the antenna is above 90%, and the gain is above 3.54 dBi in the range of 27 to 29 GHz. The peak gain is 4.3 dBi at 27 GHz.

3.2. Broadband BGA-Via Vertical Transition

BGA-via transition exhibits wider bandwidth and better electromagnetic shielding [29]. The antenna element is fed by the 50 Ω grounded coplanar waveguide (GCPW) on the system board and through the vertical quasi-coaxial BGA-via transition to the top metal layer.

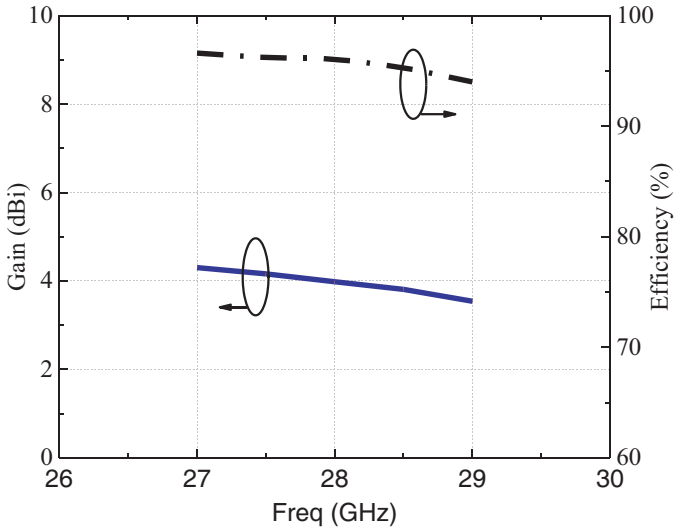

Figure 3. Simulated gain and efficiency of the proposed antenna element.

The antenna element has two vertical transitions. One is based on BGA solder balls, which are composed of RF solder balls and surrounding grounded solder balls. The other is the PTH based on GSG transition. The E-field distribution of the antenna at 28 GHz is shown in Figure 4. It can be seen that the RF signal is transmitted from the bottom solder ball to the top GSG through the PTH and is transferred to SIW by a taper transition. Then, it feeds the dipole patches. The E-field is strictly limited in the broadband BGA-via vertical transition and no electromagnetic leakage.

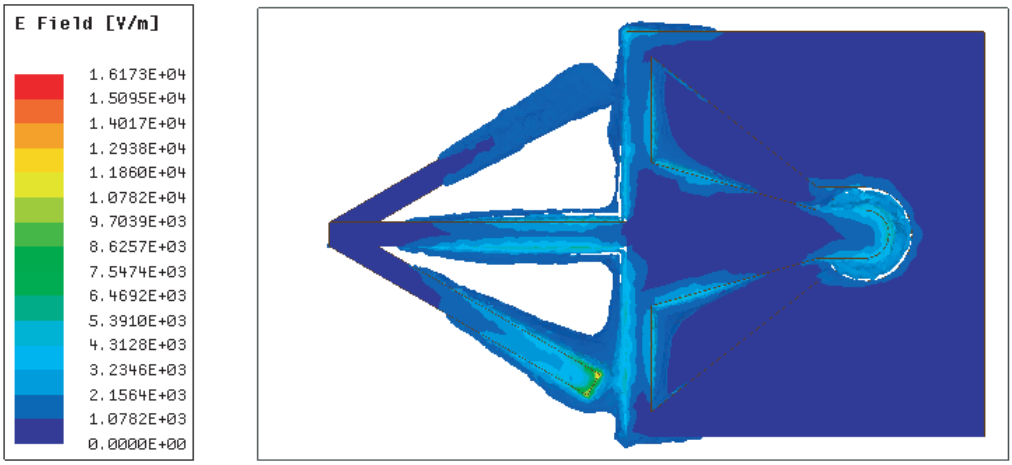

Figure 4. E-field distribution of the antenna element at 28 GHz.

3.3. Beamforming Performance

Figure 5 shows the simulated E-plane radiation pattern of a 1×8 array with different scanning angles at 28 GHz. The spacing between adjacent antenna elements is set to 4.5 mm. Besides, the input impedance of the 1×8 array is 50 Ω. The feed amplitude of the eight antenna elements is the same, but the phase depends on the scanning angle. The array scans from $-45°$ to $45°$ in steps of $15°$. It can be seen that the 3 dB beamwidth is about $14°$, and the sidelobe level is less than 12.5 dB.

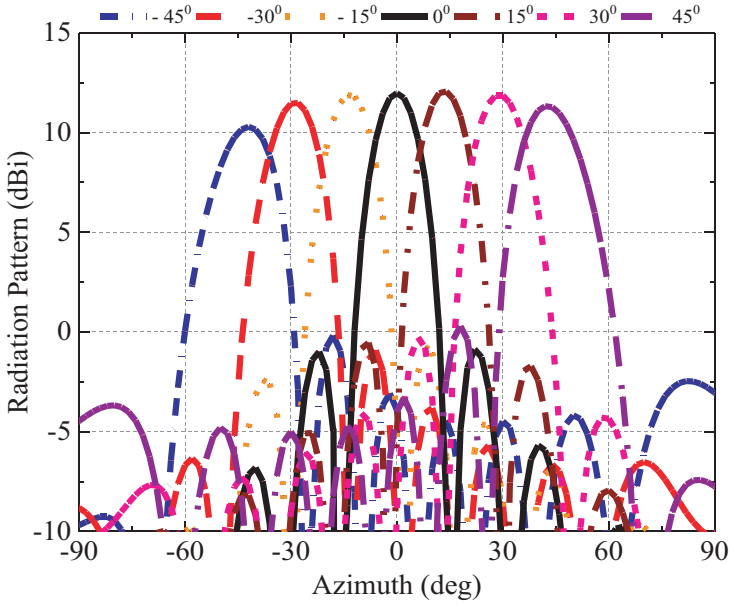

Figure 5. Simulated radiation pattern of 1×8 arrays in different scanning angles.

3.4. Manufacturing Process

The antenna substrate is fabricated using standard PCB technology. Single-layer printed circuit board processing mainly includes drilling, electroplating, resin plug hole, etching, solder mask, and gold plating. The shape accuracy of the substrate is 0.15 mm. The machining accuracy of metal is 20 microns. The solder balls are reflow soldered on the bottom layer after the PCB processing is completed. The detailed process steps are shown in Figure 6 and illustrated in detail below.

A. Drill holes on the PCB.
B. The first electroplating of metallic copper.
C. Plug the hole with resin at the drilling position.
D. The second electroplating of metallic copper.
E. Etch metal copper to form the required metal pattern.
F. Make a solder mask.
G. The PCB surface is electroplated with nickel and gold.
H. Implant the ball on the PCB substrate.

Based on the above-mentioned single-layer PCB processing technology, the manufactured antenna substrate has a good consistency and compact size. The substrate material is Rogers 4350B, which is suitable for millimeter-wave applications with low dielectric loss.

4. MEASUREMENT RESULTS AND DISCUSSION

According to the manufacturing process, a prototype is fabricated to verify the antenna performance. Photographs of the antenna prototype are shown in Figure 7. An external evaluation board is also made on Rogers4350B. Furthermore, a 50 Ω GCPW feedline is designed on the evaluation board with a width of 0.54 mm and a gap of 0.43 mm. The antenna prototype is mounted on the evaluation board by a reflow-soldering process. The S-parameters of the prototype are measured by Rohde & Schwarz Network Analyzer ZVA40. Besides, the radiation patterns are measured in the far-field anechoic chamber.

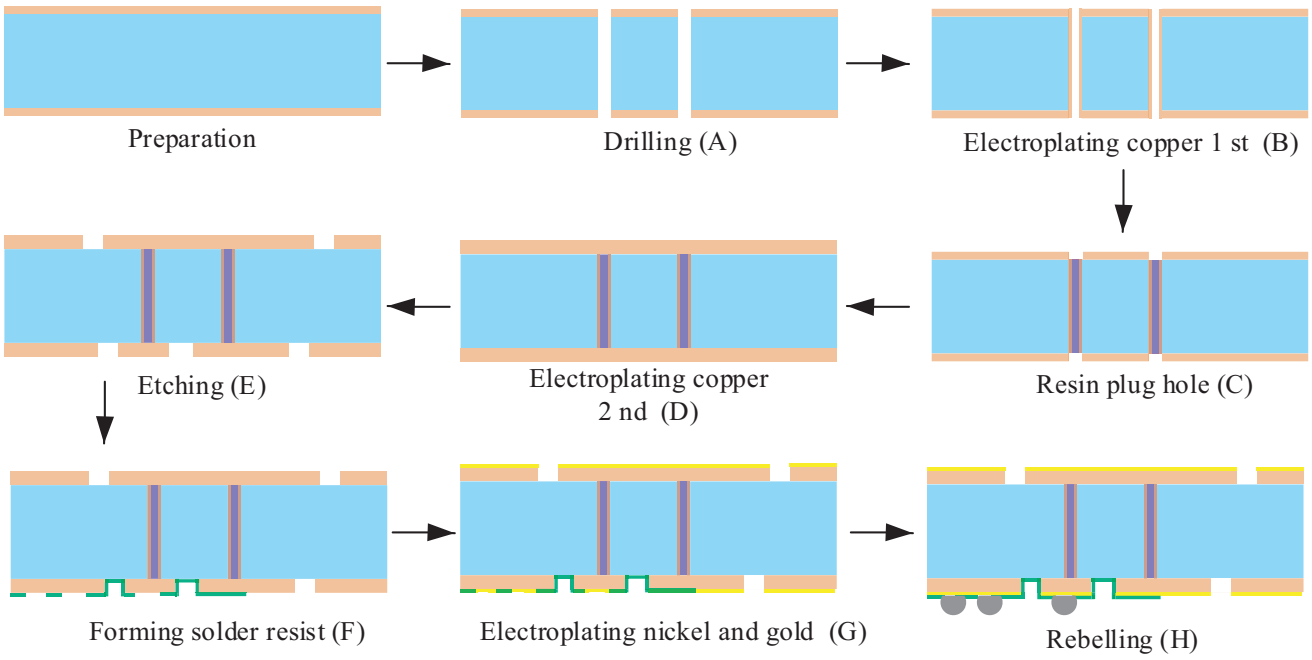

Figure 6. Manufacture process of the proposed antenna element.

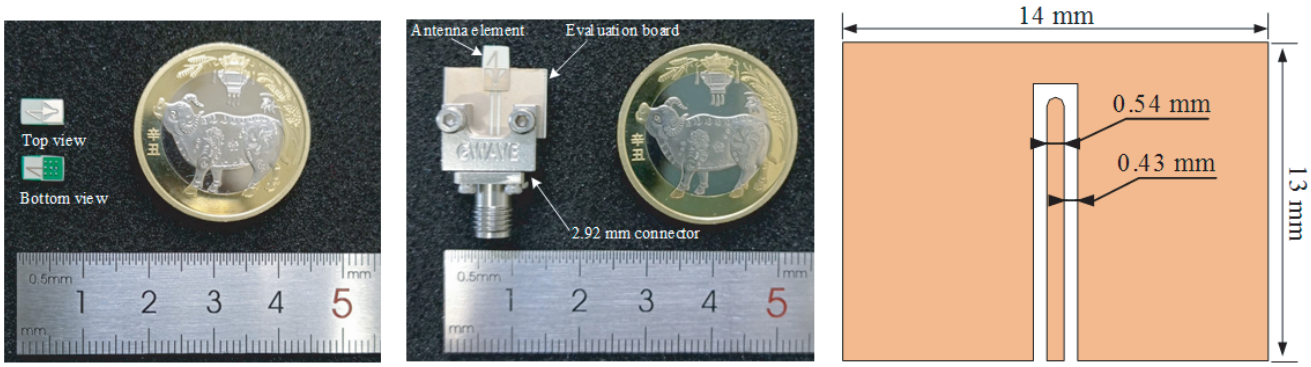

Figure 7. Photograph of the fabricated prototype. (a) Antenna element. (b) Assembled antenna element. (c) Evaluation board.

4.1. Measured Results

The measured and simulated $|S_{11}|$ and the peak gain of the antenna prototype are shown in Figure 8 and Figure 9, respectively. The simulated impedance bandwidth of $|S_{11}| < -10$ dB is 5.39% (from 27.1 to 28.6 GHz), while the measured impedance bandwidth for $|S_{11} < -10$ dB is 5.35% (from 27.3 to 28.8 GHz). The simulated gain is higher than 3.81 dBi in the range of 27 to 29 GHz, and the peak gain is 4.45 dBi at 29 GHz. Besides, the measured gain is higher than 3.48 dBi, and the peak gain is 4.4 dBi at 29 GHz. Figure 10 shows the measured and simulated normalization radiation patterns of the prototype at 27.5, 28, and 28.5, respectively.

Some discrepancies can be observed between the simulated and measured results. First, the discrepancy between the measured and simulated $|S_{11}$ is mainly due to the fabrication tolerance. As mentioned in the manufacturing processing, the fabricated accuracy may cause deviations between the actual and design values. The physical size deviation is very sensitive to the performance of the

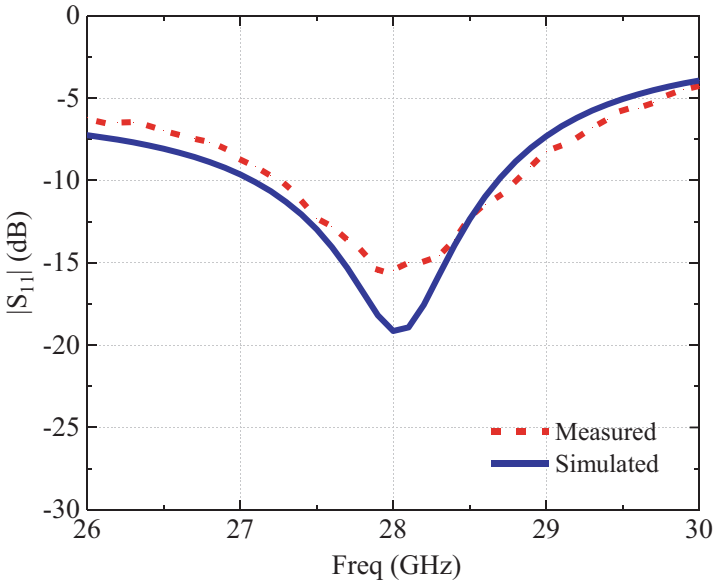

Figure 8. Measured and simulated $|S_{11}|$ of the prototype.

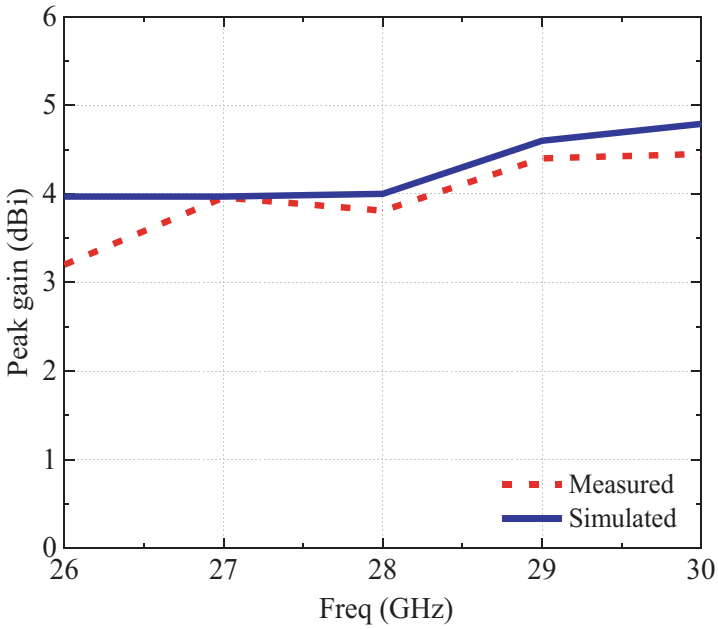

Figure 9. Measured and simulated gain of the prototype.

millimeter-wave antenna. Second, the antenna gain in Figure 9 is slightly higher than that in Figure 3. The deviation is caused by the evaluation board and 2.92 mm connector. The evaluation board and connector can be regarded as external reflectors, which can increase the antenna gain.

4.2. Comparison and Discussion

Table 2 presents the comparison between the proposed antenna and reported antennas. The main parameters are listed in the table. It can be noted that the antennas in [10, 11] must be interconnected with the RF chipsets using coaxial or waveguide connectors. The connector is bulky and lossy, which

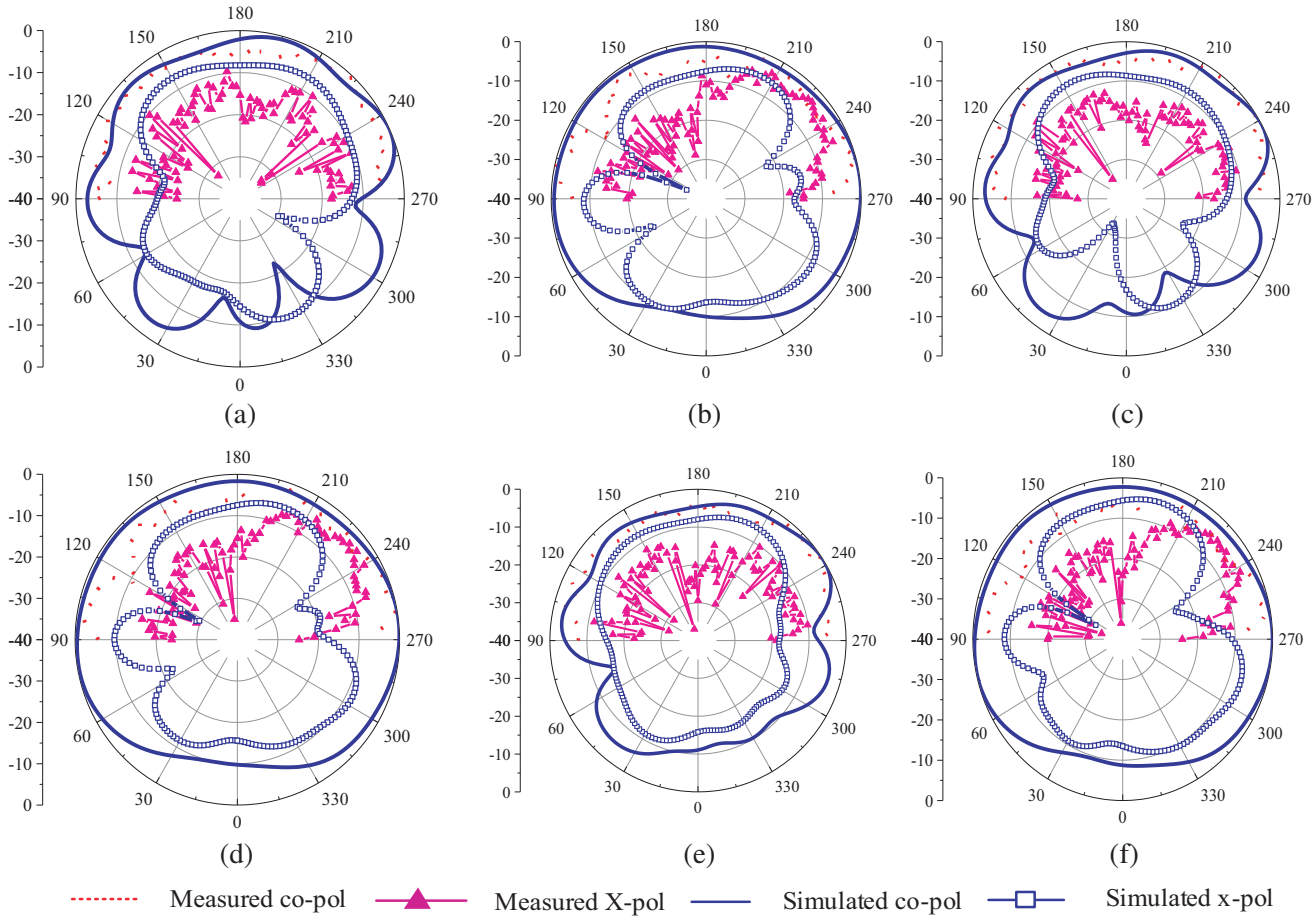

Figure 10. Measured and simulated normalization radiation patterns of the antenna prototype. (a) $f = 27.5$ GHz, E-plane. (b) $f = 27.5$ GHz, H-plane. (c) $f = 28$ GHz, E-plane. (d) $f = 28$ GHz, H-plane. (e) $f = 28.5$ GHz, E-plane. (f) $f = 28.5$ GHz, H-plane.

Table 2. Comparisons between the proposed and reported antennas.

Ref.	Center Freq. (GHz)	Element Volume ($\lambda_0 \times \lambda_0 \times \lambda_0$)	Imp. Bw	Gain (dBi)	Process technology
[10]	27.915	$0.22 \times 0.19 \times 0.11$	2.14	4.54	PCB (4 layers)
[11]	27.9	$2.79 \times 1.85 \times 0.07$	8.6	7.41	PCB (1 layer)
[17]	28.62	$0.33 \times 0.29 \times 0.07$	2.4	13.78 #	Metal Milling
[18]	34.25	$0.78 \times 0.72 \times 0.41$	21.9	8	Metal Milling
[22]	38.12	$0.69 \times 0.23 \times 0.11$	9.9	2.43	LTCC (8 layers)
This work	28.05	$0.55 \times 0.32 \times 0.06$	5.35	4.4	PCB (1 layer)

1×8 array

makes it very difficult to integrate with other devices. The proposed antenna and the antennas in [16, 17, 21] are surface-mount antennas. A surface-mount antenna is compact in size and easy to integrate with the RF front-end chipsets without the lossy waveguide connectors or coaxial lines. Compared with the metal milling technology in [16, 17], the proposed antenna uses mature PCB technology, thereby maintaining higher mechanical accuracy. Compared to the multilayer LTCC

technology in [21], the single-layer configuration shows more cost-effective potential for the massive application. In particular, the standard BGA packaging can also be automatically assembled with other discrete devices for the 5G SiP.

5. CONCLUSIONS

A 28 GHz compact BGA packaged end-fire antenna element on a single-layer substrate is proposed. The antenna prototype has been manufactured and verified. Experimental results show that the antenna element has the potential to be used in the 5G NR mmWave frequency band (n257 26.5–29.5 GHz; n261 27.5–28.35 GHz). Besides, the single-layer configuration shows cost-effective features for large-scale applications. Besides, due to the application of compact BGA packaging, the antenna element is easily integrated into the RF SiP. Therefore, the proposed antenna element will be attractive for 5G mmWave NR systems.

ACKNOWLEDGMENT

The authors would like to thank Prof. Hongxing Zheng of the School of Electronics and Information Engineering, Hebei University of Technology, for helping with the antenna measurements.

REFERENCES

1. Pi, Z. and F. Khan, "An introduction to millimeter-wave mobile broadband systems," *IEEE Commun. Mag.*, Vol. 49, No. 6, 101–107, Jun. 2011.
2. Andrews, J. G., et al., "What will 5G be?," *IEEE J. Sel. Areas Commun.*, Vol. 32, No. 6, 1065–1082, Jun. 2014.
3. Rappaport, T. S., et al., "Millimeter wave mobile communications for 5G cellular: It will work!," *IEEE Access*, Vol. 1, 335–349, 2013.
4. Hong, W., K. Baek, and S. Ko, "Millimeter-wave 5G antennas for smartphones: Overview and experimental demonstration," *IEEE Trans. Antennas Propag.*, Vol. 65, No. 12, 6250–6261, Dec. 2017.
5. Ying, Z., "Antennas in cellular phones for mobile communications," *Proc. IEEE*, Vol. 100, No. 7, 2286–2296, Jul. 2012.
6. Roh, W., et al., "Millimeter-wave beamforming as an enabling technology for 5G cellular communications: Theoretical feasibility and prototype results," *IEEE Commun. Mag.*, Vol. 52, No. 2, 106–113, Feb. 2014.
7. Hong, W., K. Baek, Y. Lee, Y. Kim, and S. Ko, "Study and prototyping of practically large-scale mmWave antenna systems for 5G cellular devices," *IEEE Commun. Mag.*, Vol. 52, No. 9, 63–69, Sep. 2014.
8. Yin, J., Q. Wu, C. Yu, H. Wang, and W. Hong, "Broadband endfire magnetoelectric dipole antenna array using SICL feeding network for 5G millimeter-wave applications," *IEEE Trans. Antennas Propag.*, Vol. 67, No. 7, 4895–4900, Jul. 2019.
9. Mak, K.-M., K.-K. So, H.-W. Lai, and K.-M. Luk, "Magnetoelectric dipole leaky-wave antenna for millimeter-wave application," *IEEE Trans. Antennas Propag.*, Vol. 65, No. 12, 6395–6402, Dec. 2017.
10. Tang, M., T. Shi, and R. W. Ziolkowski, "A study of 28 GHz, planar, multilayered, electrically small, broadside radiating, huygens source antennas," *IEEE Trans. Antennas Propag.*, Vol. 65, No. 12, 6345–6354, Dec. 2017.
11. Park, J., J. Ko, H. Kwon, B. Kang, B. Park, and D. Kim, "A tilted combined beam antenna for 5G communications using a 28-GHz band," *IEEE Antennas Wirel. Propag. Lett.*, Vol. 15, 1685–1688, 2016.

12. Yu, B., K. Yang, C.-Y.-D. Sim, and G. Yang, "A novel 28 GHz beam steering array for 5G mobile device with metallic casing application," *IEEE Trans. Antennas Propag.*, Vol. 66, No. 1, 462–466, Jan. 2018.
13. Karthikeya, G. S., M. P. Abegaonkar, and S. K. Koul, "CPW-fed all-metallic Vivaldi antennas with pattern diversity for millimeter wave 5G access points," *Progress In Electromagnetics Research M*, Vol. 94, 41–49, 2020.
14. Watanabe, A. O., M. Ali, S. Y. B. Sayeed, R. R. Tummala, and M. R. Pulugurtha, "A review of 5G front-end systems package integration," *IEEE Trans. Compon. Packag. Manuf. Technol.*, Vol. 11, No. 1, 118–133, Jan. 2021.
15. Zhang, Y., "Antenna-in-package technology: Its early development [historical corner]," *IEEE Antennas Propag. Mag.*, Vol. 61, No. 3, 111–118, Jun. 2019.
16. Zhang, Y. and J. Mao, "An overview of the development of antenna-in-package technology for highly integrated wireless devices," *Proc. IEEE*, Vol. 107, No. 11, 2265–2280, Nov. 2019.
17. Park, J., D. Choi, and W. Hong, "Millimeter-wave phased-array Antenna-in-Package (AiP) using stamped metal process for enhanced heat dissipation," *IEEE Antennas Wirel. Propag. Lett.*, Vol. 18, No. 11, 2355–2359, Nov. 2019.
18. Ahmad, Z. and J. Hesselbarth, "High-efficiency wideband surface-mount elevated 3-D patch antenna for millimeter waves," *IEEE Antennas Wirel. Propag. Lett.*, Vol. 16, 573–576, 2017.
19. Lin, W., R. W. Ziolkowski, and T. C. Baum, "28 GHz compact omnidirectional circularly polarized antenna for device-to-device communications in the future 5G systems," *IEEE Trans. Antennas Propag.*, Vol. 65, No. 12, 6904–6914, Dec. 2017.
20. Hong, W., K.-H. Baek, and A. Goudelev, "Multilayer antenna package for IEEE 802.11ad employing ultralow-cost FR4," *IEEE Trans. Antennas Propag.*, Vol. 60, No. 12, 5932–5938, Dec. 2012.
21. Liu, D., X. Gu, C. W. Baks, and A. Valdes-Garcia, "Antenna-in-package design considerations for Ka-band 5G communication applications," *IEEE Trans. Antennas Propag.*, Vol. 65, No. 12, 6372–6379, Dec. 2017.
22. Park, J., H. Seong, Y. N. Whang, and W. Hong, "Energy-efficient 5G phased arrays incorporating vertically polarized endfire planar folded slot antenna for mmWave mobile terminals," *IEEE Trans. Antennas Propag.*, Vol. 68, No. 1, 230–241, Jan. 2020.
23. Zhang, Y. P., "Integration of microstrip patch antenna on ceramic ball grid array package," *Electron. Lett.*, Vol. 38, No. 5, 207–208, Feb. 2002.
24. Zhang, Y. P., M. Sun, K. M. Chua, L. L. Wai, and D. X. Liu, "Integration of slot antenna in LTCC package for 60 GHz radios," *Electron. Lett.*, Vol. 44, No. 5, 330–331, Feb. 2008.
25. Sun, M., Y. P. Zhang, K. M. Chua, L. L. Wai, D. Liu, and B. P. Gaucher, "Integration of Yagi antenna in LTCC package for differential 60-GHz radio," *IEEE Trans. Antennas Propag.*, Vol. 56, No. 8, 2780–2783, Aug. 2008.
26. Watanabe, A. O., et al., "3D glass-based panel-level package with antenna and low-loss interconnects for millimeter-wave 5G applications," *2019 IEEE MTT-S International Microwave Conference on Hardware and Systems for 5G and Beyond (IMC-5G)*, 1–3, Aug. 2019.
27. Jin, C., V. N. Sekhar, X. Bao, B. Chen, B. Zheng, and R. Li, "Antenna-in-package design based on wafer-level packaging with through silicon via technology," *IEEE Trans. Compon. Packag. Manuf. Technol.*, Vol. 3, No. 9, 1498–1505, Sep. 2013.
28. Huang, Y. and K. Boyle, *Antennas: From Theory to Practice*, 379, 2008.
29. Kangasvieri, T., J. Halme, J. Vahakangas, and M. Lahti, "Broadband BGA-via transitions for reliable RF/Microwave LTCC-SiP module packaging," *IEEE Microw. Wirel. Compon. Lett.*, Vol. 18, No. 1, 34–36, Jan. 2008.